Bioorg. Med. Chem. Lett. 36 (2021) 127786

Contents lists available at ScienceDirect

Bioorganic & Medicinal Chemistry Letters

journal homepage: www.elsevier.com/locate/bmcl

Discovery of 6-Oxo-4-phenyl-hexanoic acid derivatives as RORγt inverse agonists showing favorable ADME profile

Ryota Nakajima [a,1,*], Hiroyuki Oono [a], Keiko Kumazawa [a], Tomohide Ida [a], Jun Hirata [a], Ryan D. White [b], Xiaoshan Min [c], Angel Guzman-Perez [b], Zhulun Wang [c], Antony Symons [d], Sanjay K. Singh [e,2], Srinivasa Reddy Mothe [e,3], Sergei Belyakov [e,4], Anjan Chakrabarti [e,5], Satoshi Shuto [f,g,*]

[a] Teijin Institute for Bio-medical Research, Teijin Pharma Limited, 4-3-2 Asahigaoka, Hino, Tokyo 191-8512, Japan
[b] Department of Medicinal Chemistry, Amgen Discovery Research, Amgen Inc., 360 Binney Street, Cambridge, MA 02142, United States
[c] Departments of Molecular Engineering, Amgen Discovery Research, Amgen Inc., 1120 Veterans Boulevard, South San Francisco, CA 94080, United States
[d] Departments of Inflammation & Oncology Research Amgen Inc., 1120 Veterans Boulevard, South San Francisco, CA 94080, United States
[e] AMRI Singapore Research Centre, Pte. Ltd., 61 Science Park Road, #05-01 The Galen, Science Park III, Singapore 117525, Singapore
[f] Faculty of Pharmaceutical Sciences, Hokkaido University, Kita-12, Nishi-6, Kita-ku, Sapporo 060-0812, Japan
[g] Center for Research and Education on Drug Discovery, Hokkaido University, Kita-12, Nishi-6, Kita-ku, Sapporo 060-0812, Japan

ARTICLE INFO

Keywords:
Nuclear receptor
RORγt
Inverse agonist

ABSTRACT

The retinoic acid receptor-related orphan nuclear receptor gamma t (RORγt), which is a promising therapeutic target for immune diseases, is a major transcription factor of genes related to psoriasis pathogenesis, such as interleukin (IL)-17A, IL-22, and IL-23R. Inspired by the co-crystal structure of RORγt, a 6-oxo-4-phenyl-hexanoic acid derivative **6a** was designed, synthesized, and identified as a ligand of RORγt. The structure–activity relationship (SAR) studies in **6a**, which focus on the improvement of its membrane permeability profile by introducing chlorine atoms, led to finding **12a,** which has a potent RORγt inhibitory activity and a favorable pharmacokinetic profile.

The retinoic acid receptor-related orphan nuclear receptor gamma t (RORγt) is a major transcription factor of genes related to psoriasis pathogenesis, such as interleukin (IL)-17A, IL-22, and IL-23R.[1–2] Therapies that block IL-17A or IL-23R have successfully improved the skin lesions of patients with moderate-to-severe psoriasis,[3–7] thus rendering RORγt inhibition as a promising therapeutic target. Many RORγt antagonists (inverse agonists) have been developed,[8–23] and some of them are now being clinically investigated for the treatment of autoimmune diseases.[24] Generally, nuclear receptors have high conserved ligand-binding domains (LBDs), which are structurally composed of alpha helices that form large lipophilic pockets responsible for the binding of small lipophilic ligands, such as retinoid derivatives, fatty acids, cholesterol, and other lipophilic hormones and vitamins.[25] Thus, hydrophobicity balance is one of the main challenges for drug delivery in this target class, as hydrophobicity is essential for strong LBD binding potency. However, it should also be minimized to avoid undesirable metabolisms for the favorable drug-like properties in small-molecule ligands (Fig 1.).

In 2014, a novel RORγt inverse agonist **1** with a basic piperazine ring was disclosed by GSK.[26] Using **1** as a lead, we reported triazolopyridine

Abbreviations: BA, bioavailability; RORγt, retinoic acid receptor-related orphan receptor γt.

* Corresponding authors at: Teijin Limited, 2-1, Kasumigaseki 3-chome, Chiyoda-ku, Tokyo 100-8585, Japan (R. Nakajima). Faculty of Pharmaceutical Sciences, Hokkaido University, Kita-12, Nishi-6, Kita-ku, Sapporo 060-0812, Japan (S. Shuto).
E-mail addresses: r.nakajima@teijin.co.jp (R. Nakajima), shu@pharm.hokudai.ac.jp (S. Shuto).
[1] Present address: Teijin Limited, 2-1, Kasumigaseki 3-chome, Chiyoda-ku, Tokyo 100-8585, Japan.
[2] Present address: AWAK Technologies, 3 Tuas Lane, Singapore 638612, Singapore.
[3] Present address: Polymer Engineering Characterization, Institute of Chemical and Engineering Sciences, Agency of Science, Technology and Research, 1 Pesek Road, Jurong Island, Singapore 627833, Singapore.
[4] Present address: Wintershine Health and Skincare Pte Ltd., 23 Goldhill Pl., Singapore 308931, Singapore.
[5] Present address: Syngene International Limited, Biocon Park SEZ, Bommasandra IV Phase, Jigani Link Road, Bangalore 560099, India.

https://doi.org/10.1016/j.bmcl.2021.127786
Received 11 October 2020; Received in revised form 25 December 2020; Accepted 9 January 2021
Available online 23 January 2021

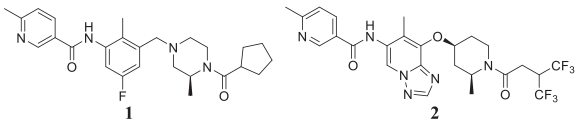

Fig. 1. An RORγt ligand used as a reference, and triazolopyridine analog reported in the former study.

analog **2** exhibiting *in vivo* RORγt inhibitory activity after its oral dosing.[27] Herein, we present a separate effort from compound **1** toward 6-oxo-4-phenyl-hexanoic acid analogs as a novel RORγt inverse agonist, which improves the PK profile compared with **1**.

According to the x-ray co-crystal structure of compound **3** (an analog of compound **1**) complexed with RORγt (PDB ID: 6O3Z),[27] a hydrogen bond between the *N*-phenylamide NH and the backbone carbonyl of Phe377 was observed. On the other hand, carboxylic acid **4** was reported by Japan Tabaco, which is a RORγt inverse agonist that has similar *N*-phenylamide moiety and hydrogen bonding with Phe377 (PDB ID: 6IVX).[28] Considering the hydrophobicity balance, the carboxylic acid moiety was desirable to decrease hydrophobicity, suggesting a replacement of the benzamide moiety of **1** or **3** by the 4-aryl-hexanoic acid moiety of **4** (Fig. 2B).

Therefore, we synthesized several analogs of **1** bearing 6-oxo-4-aryl-hexanoic acid moiety, which were evaluated using a RORγt binding assay (cell-free system) and a RORγt luciferase reporter gene assay (cell-based system). The SAR results of the benzamide moiety modifications in compound **1** are summarized in Table 1.

As outlined in Table 1, the $cLogD_{7.4}$ values of the novel analogs were decreased compared with **1** by introducing carboxylic acid moieties (**5a**, **5b**, **6a**, **6b**, **7a**, **7b** and **8**). The thiazole-hexanoic acid analogs **5a** and **5b** showed an excellent RORγt binding activity, but its relatively lower transcriptional inhibitory activity was observed (IC_{50} = 63 nM vs 1400 nM for the diastereomer **5a**, IC_{50} = 110 nM vs 1100 nM for the diastereomer **5b**). The phenyl-hexanoic acid analogs **6a** and **6b** exhibited an increased transcriptional inhibitory activity in addition to an improved liver microsomal stability, but a similar discrepancy between the binding affinity for RORγt and the inhibitory effect in the cells was observed. The truncated analogs **7a**, **7b** and **8** showed a decreased binding affinity and a transcriptional inhibitory activity, which indicated that the lengths of the alkyl chain and aryl ring at the 4-position of alkyl acid moiety are important for the RORγt inhibitory effect. Thus, a similar discrepancy between the binding affinity and transcriptional inhibitory effects was observed for these carboxylic acid analogs (**6a**, **6b**, **7a**, **7b** and **8**). However, the 3-phenylpropanamide analog **9** did not show such a discrepancy although its microsomal stability was decreased. The phenyl-hexanoic acid analog **6a** showed an improved binding affinity and microsomal stability compared with the parent compound **1**, and it served as a new starting point for further optimization to improve inhibitory activity. The relatively lower activity in the cells suggested that the alkyl carboxylic acid analogs had a low membrane permeability. Therefore, several analogs of **6** were designed and prepared to focus on improving the permeability profile, and the results of their biological evaluations were summarized, as shown in Table 2.

Table 1
Structure-activity relationships (SAR) of the benzamide moiety modifications in compound **1**

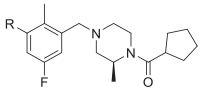

Compound	R[a]	$cLogD_{7.4}$[b]	Binding IC_{50} (nM)[c]	Luc IC_{50} (nM)[d]	Human LM CL_{int} (mL/min/mg)[e]
1	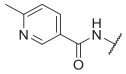	3.8	59	17	0.088
5a	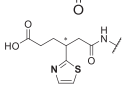	2.2	63	1400	
5b			110	1100	
6a	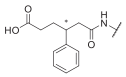	3.6	44	120	<0.010
6b			52	160	0.021
7a	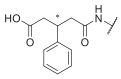	3.1	2100	15,000	
7b			1800	6500	
8	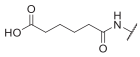	0.82	330	2500	
9		5.1	67	99	1.9

[a] The absolute stereochemistry at the branched tertiary carbon (*) in **5a**, **5b**, **6a**, **6b**, **7a** and **7b** remained unknown.
[b] Calculated by Pipeline Pilot 17.2.
[c] Binding assay.
[d] Luciferase reporter gene assay used for the evaluation of the RORγt transcriptional activity inhibition (The employed HEK293T cells were transfected with GAL4-NR-luciferase plasmids, and the activity was evaluated using the Dual-GLOTM luciferase assay system.).
[e] Metabolic stability in the liver microsome (LM).

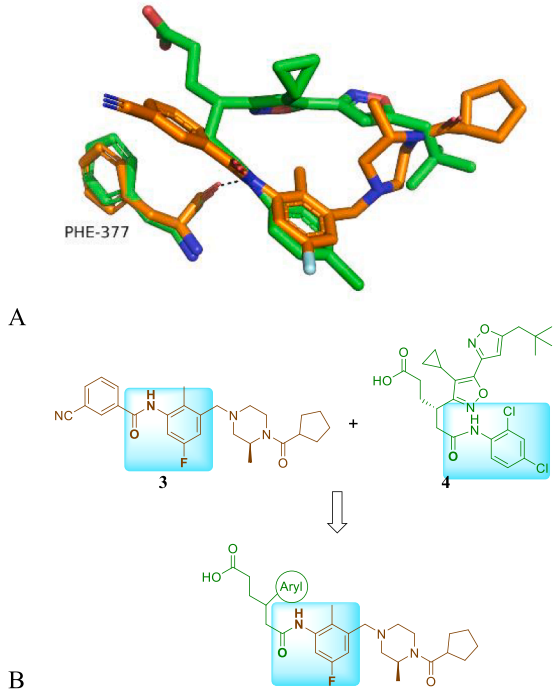

Fig. 2. (A) Superimposed RORγt binding conformations of **3** (PDB ID: 6O3Z) and **4** (PDB ID: 6IVX) (**3**: orange color by atom; **4**: green color by atom); Phe377 from the corresponding RORγt crystal structures are shown, colored as **3** and **4**; The overlay is based on the superposition of the RORγt LBD in the crystal structures of the two complexes; (B) Compound design inspired from the superimposed conformations of **3** and **4**.

The x-ray co-crystal structure of compound **3** complexed with RORγt described a space around the fluorobenzene of **3**[27], which motivated us to replace fluorine atom to chlorine atom for balancing hydrophobicity and permeability. Furthermore, the piperazine ring of **6** was replaced by a piperidine ring to avoid the formation of a zwitterionic structure, resulting in the derivatives **10a** and **10b**. Though $cLogD_{7.4}$ values for **10a** and **10b** were increased ($cLogD_{7.4}$ = 4.1 for **10a** and **10b**), the transcriptional inhibitory activity were not improved compared with **6a** (Luc IC_{50} = 280 nM for **10a** and Luc IC_{50} = 410 nM for **10b**). Then, we focused on the amide NH proton, as the hydrogen bonding donors in the drug molecule can have a deleterious effect on the membrane

Table 2

SAR of the **6a** derivatives.

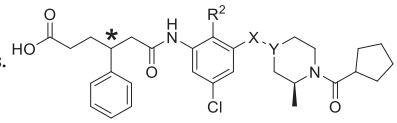

Compound [a]	R^2		$cLogD_{7.4}$ [b]	Binding IC_{50} (nM) [c]	Luc IC_{50} (nM) [d]	Human LM CL_{int} (mL/min/mg) [e]
10a	Me		4.1	100	280	
10b			4.1	170	410	
11a	Cl		4.3	54	31	0.016
11b			4.3	51	45	
12a	Cl		4.2	35	19	0.031
12b			4.2	34	25	<0.010

[a] The absolute stereochemistry at the branched tertiary carbon (*) in **10a**, **10b**, **11a**, **11b**, **12a,** and **12b** remained unknown.
[b] Calculated by Pipeline Pilot 17.2.
[c] Binding assay.
[d] Luciferase reporter gene assay used for the evaluation of the RORγt transcriptional activity inhibition (The employed HEK293T cells were transfected with GAL4-NR-luciferase plasmids, and the activity was evaluated using the Dual-GLOTM luciferase assay system.).
[e] Metabolic stability in the liver microsome (LM).

penetration. Although the intramolecular hydrogen bond in the 2-chloro aniline structure was not reported, introducing chloride to **6** might affect the properties of amide NH, which potentially improves the membrane permeability. Thus, the compounds **11a**, **11b**, **12a** and **12b**, in which the methyl group on the aniline moiety of **6a** was replaced by a chlorine atom, were designed and prepared. To our delight, these analogs exhibited a retained binding activity and improved the transcriptional inhibitory activity with a good liver microsomal stability compared with **6a**.

The representative compounds **1**, **6a**, **11a** and **12a** in the series were selected for ADME evaluation, and the results were recorded, as shown in Table 3. Compared with compound **1**, all the newly evaluated compounds showed an excellent liver microsomal stability and a similar high plasma protein binding (PPB) feature. Notably, a low caco-2 permeability in the apical-to-basolateral (A to B) direction and a high efflux ratio were observed for the compound **6a** (Caco-2 efflux ratio = 30). However, the compounds **11a** and **12a** exhibited an improved permeability profile in the same evaluation system (Caco-2 efflux ratio = 2.6 for **11a** and 3.5 for **12a**). The *in vivo* PK profile of the compounds was investigated in mice using cassette dosing. Compounds **11a** and **12a** showed improved bioavailability (>86%), clearance (<0.52 L/h/kg), area under the curve (AUC) (>4000 nM*h), and $t_{1/2}$ (>1.5 h) compared with compound **6a**.

To understand the binding mode of **11a** and **12a** in RORγt LBD, we carried out co-crystallization studies of **11a** with RORγt LBD. The crystal structure of RORγt LBD in complex with **11a** was obtained at 1.9 A resolution (PDB ID: 7JTW), as shown in Figure 3. The NH of the amide moiety formed a hydrogen bond with the backbone carbonyl of Phe377. The phenyl ring of the hexanoic acid occupied a pocket surrounded by His323, Met365, and Ala327. The carboxylic acid portion extended out toward the solvent-exposed region, forming a hydrogen bond interaction with the backbone amide of Glu379.

The synthetic route to the representative piperazine derivatives **5a**, **5b**, **6a** and **6b** is shown in Scheme 1. Compounds **17** and **18** were synthesized using the Horner-Emmons reaction of **13** and **14** followed by the deprotection of **15** and **16**. Then, the olefin moiety was hydrogenated by Pd/C under an H_2 atmosphere to obtain **19** and **20**. The synthesis of **5** and **6** was achieved by subjecting **19** and **20** to amidation, followed by deprotection and then chiral separation, to provide diastereomers a (early eluting) and diastereomers b (late eluting), respectively.

Scheme 2 depicts the synthetic route to **10**. The Mitsunobu reaction of the phenol derivative **23** followed by the saponification of **24** afforded **25**. Then, **26** was prepared by the Curtius reaction of **25**. The final compound **10** was synthesized using amidation, subsequent hydroxylation, and chiral SFC separation in a similar manner to Scheme 1 to obtain the diastereomers a (early eluting) and diastereomers b (late eluting). The preparation of the other piperazine and piperidine analogs is detailed in the Supplementary Information section.

In summary, a new 6-oxo-4-phenyl-hexanoic acid analog **6a** was identified as a potent RORγt inhibitor. The optimization of the membrane permeability profile led to the novel analogs **11a** and **12a**, which exhibited a potent RORγt inhibitory activity in the luciferase reporter gene assay as well as a robust *in vitro/in vivo* ADME profile. Furthermore, the binding mode of **11a** was clarified using x-ray analysis with the co-crystal with RORγt LBD.

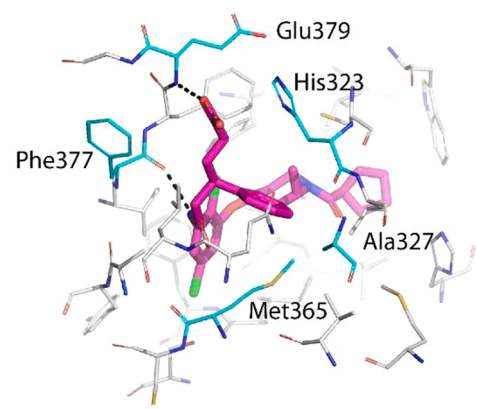

Fig. 3. Crystal structure of **11a** in RORγt LBD (PDB ID: 7JTW) (The absolute stereochemistry of **11a** obtained from this x-ray structure indicated that the absolute configuration of the chiral center at the 4-position of hexanoic acid was R.)

Table 3
ADME profiles of the compounds **1**, **5a**, **11a** and **12a.**

Compound	LM CL_{int} (mL/min/mg) [a]		PPB (%) [b]		Caco-2 P_{app} ($\times 10^{-6}$cm/s) [c]			[d] Mice cassette dosing study			
	human	mouse	human	mouse	A to B	B to A	Efflux ratio	BA (%)	AUC p.o. (nM*h)	CL(L/h/kg)	$t_{1/2}$ (h)i.v. / p.o.
1	0.088	0.11	99.7	95.7	40	55	1.4	48	490	2.0	0.7/0.7
6a	<0.010	0.017	99.4	97.2	1.3	39	30	46	200	4.6	1.2/1.5
11a	0.016	<0.010	99.4	99.5	16	41	2.6	86	4800	0.36	2.3/1.9
12a	0.031	<0.010	99.7	99.4	13	45	3.5	100	4000	0.52	1.5/1.5

[a] Metabolic stability in the liver microsome.
[b] Plasma protein binding using human or mouse plasma.
[c] Permeability in the apical-to-basolateral (A to B) direction and *vice versa* (B to A) and the efflux ratio.
[d] 2 μmol/kg p.o. dose and 1 μmol/kg i.v. dose.

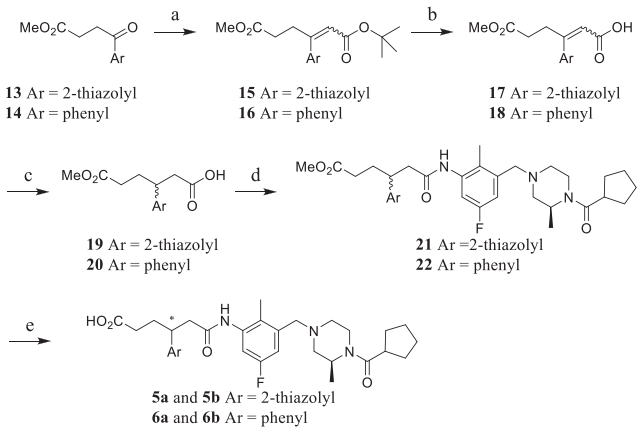

Scheme 1. Synthesis of the representative piperazine derivatives[a]. [a]Reaction conditions: a) NaH, *tert*-butyl 2-(diethoxyphosphoryl)acetate, THF, 0 °C; b) 4 *N* HCl in dioxane, 0 °C, rt; c) H_2, 10% Pd/C, THF, MeOH; d) Oxalyl chloride, DMF, CH_2Cl_2, 0 °C; then (S)-(4-(3-amino-5-fluoro-2-methylbenzyl)-2-methylpiperazin-1-yl)(cyclopentyl)methanone[26], TEA, CH_2Cl_2, 0 °C; e) LiOH, THF, MeOH, H_2O, chiral column SFC separation (AD-H column for **5**, IA column for **6**).

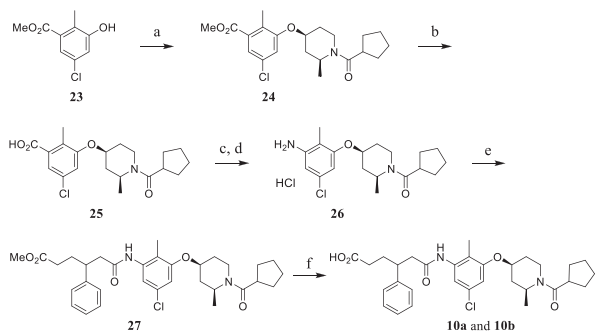

Scheme 2. Synthesis of the representative piperidine derivatives **10a** and **10b**[a]. [a]Reaction conditions: a) Tsunoda reagent, cyclopentyl((2S)-4-hydroxy-2-methylpiperidin-1-yl)methanone, toluene, 110 °C, chiral column SFC separation (AD-H column); b) LiOH, THF, MeOH, H_2O; c) DPPA, DIPEA, *tert*-BuOH, 100 °C; d) 4 *N* HCl in dioxane; e) Oxalyl chloride, DMF, 20, CH_2Cl_2, 0 °C; then added to **26**, TEA, CH_2Cl_2, 0 °C; f) LiOH, MeOH, H_2O, chiral column SFC separation (AD-H column).

Declaration of Competing Interest

The authors declare that they have no known competing financial interests or personal relationships that could have appeared to influence the work reported in this paper.

Acknowledgments

We thank Ryo Matsuyama, Mariko Hirano, Atsushi Baba, Emi Yokoyama and Akiko Takeuchi for the pharmacological discussion. We thank Steve Thibault and Haoda Xu for the protein supply.

Appendix A. Supplementary data

Supplementary data (Synthetic experimental, compound characterization, crystallography studies and assay descriptions) to this article can be found online at https://doi.org/10.1016/j.bmcl.2021.127786. These data include MOL files and InChiKeys of the most important compounds described in this article.

References

1 Ivanov II, McKenzie BS, Zhou L, et al. *Cell*. 2006;126:1121–1133.
2 Annunziato F, Cosmi L, Santarlasci V, et al. *J Exp Med*. 2007;204:1849–1861.
3 Hueber, W., Patel, D. D., Dryja, T., et al., Sci Transl Med 2010, 2, 52ra72.
4 Leonardi C, Matheson R, Zachariae C, et al. *N Engl J Med*. 2012;366:1190–1199.
5 Langley, R. G., Elewski, B. E., Lebwohl, M., et al., N Engl J Med 2014, 371, 326-338.
6 Papp KA, Reich K, Paul C, et al. *Br J Dermatol*. 2016;175:273–286.
7 Farahnik B, Beroukhim K, Zhu TH, et al. *Dermatol Ther*. 2016;6:25–37.
8 Kumar N, Solt LA, Conkright JJ, et al. *Mol Pharmacol*. 2010;77:228–236.
9 Cyr P, Bronner SM, Crawford JJ. *Bioorg Med Chem Lett*. 2016;26:4387–4393.
10 Qiu R, Wang Y. *J Med Chem*. 2018;61:5794–5804.
11 Pandya VB, Kumar S, Sachchidanand, Sharma R, Desai RC. *J Med Chem*. 2018;61:10976–10995.
12 van Niel MB, Fauber BP, Cartwright M, et al. *Bioorg Med Chem Lett*. 2014;24:5769–5776.
13 Chao J, Enyedy I, Van Vloten K, et al. *Bioorg Med Chem Lett*. 2015;25:2991–2997.
14 Wang Y, Cai W, Cheng Y, et al. *ACS Med Chem Lett*. 2015;6:787–792.
15 Hirata K, Kotoku M, Seki N, et al. *ACS Med Chem Lett*. 2016;7:23–27.
16 Olsson RI, Xue Y, von Berg S, et al. *ChemMedChem*. 2016;11:207–216.
17 Rene O, Fauber BP, Barnard A, et al. *Bioorg Med Chem Lett*. 2016;26:4455–4461.
18 Ouvry G, Bouix-Peter C, Ciesielski F, et al. *Bioorg Med Chem Lett*. 2016;26:5802–5808.
19 Kummer DA, Cummings MD, Abad M, et al. *Bioorg Med Chem Lett*. 2017;27:2047–2057.
20 Barbay JK, Cummings MD, Abad M, et al. *Bioorg Med Chem Lett*. 2017;27:5277–5283.
21 Kono M, Ochida A, Oda T, et al. *J Med Chem*. 2018;61:2973–2988.
22 Gege C, Cummings MD, Albers M, et al. *Bioorg Med Chem Lett*. 2018;28:1446–1455.
23 Tian J, Sun N, Yu M, et al. *Eur. J. Med. Chem*. 2019;167:37–48.
24 Sun N, Guo H, Wang Y. *Expert Opin Ther Pat*. 2019;29:663–674.
25 Burris TP, Solt LA, Wang Y, et al. *Pharmacol Rev*. 2013;65:710–778.
26 Han F, Lei H, Lin X, Meng Q, Wang Y. *WO Patent WO2014/086894A1*. 2014.
27 Nakajima R, Oono H, Sugiyama S, et al. *ACS Med Chem Lett*. 2020;11:528–534.
28 Kotoku M, Maeba T, Fujioka S, et al. *J Med Chem*. 2019;62:2837–2842.